EASD
Procedia

A SYSTEMATIC INVESTIGATION OF COMMON GRADIENT BASED MODEL UPDATING APPROACHES APPLIED TO HIGH-FIDELITY TEST-DATA OF A WIND TURBINE ROTOR BLADE

Johannes Knebusch[1], Janto Gundlach[1], and Yves Govers[1]

German Aerospace Center (DLR)
Institute of Aeroelasticity
Bunsenstraße 10, 37073 Göttingen
Germany

johannes.knebusch@dlr.de
janto.gundlach@dlr.de
yves.govers@dlr.de

Keywords: Windenergy, Rotorblade, High-Fidelity, Model Updating

Abstract. *Within the context of the "SmartBlades2"-project, a wind turbine rotor blade was designed and extensively tested. The rotor-blade uses a lightweight composite structure and bend-twist coupling. The bend-twist coupling facilitates a passive load-reduction by changing the angle of attack under load. Due to a high sensor-density of 265 accelerometers in the experimental modal test of the blade, the sophisticated structural dynamics of the model are captured. Apart from the commonly measured first flapwise-, edgewise-bending and torsion mode, 35 modes up to a frequency of 60 Hz are identified. Unlike in many other wind turbine rotor blade investigations, the Finite Element (FE) model uses shell elements instead of beam elements and is directly based on production drawings. This experimental and simulative setup is particularly relevant, since a significant number of mode shapes exhibit a distinct local behavior which was in previous studies not accounted for. The differences between experimental and simulated results are minimized using computational model updating procedures. In this case-study, two formerly underrepresented aspects of the updating of large-scale FE models are examined. One is the use of different parameterizations and the other is the possibility of insufficient experimental data. The parametrizations are based on well-established criteria like error-localization and sensitivity. Moreover, the updating is performed with different (i.e. reduced) subsets of the modal data and the results are then compared to the model updating results achieved with the entire dataset. This in-depth investigation of the model updating of a composite structure allows the deduction of general guidelines in the model updating of industrial-sized FE models.*

1 INTRODUCTION

1.1 Model updating of rotor blades

In recent years a large number of wind-turbines were installed [14, 16, 19]. While the total installed power increased significantly, the output per wind turbine was also improved. This was reached by a number of measures. Aside from higher towers and efficiency improvements of the drivetrain, one important aspect is the aerodynamic improvement of the rotor blade [27]. Two closely related main trends govern this aerodynamic improvement. One is the aerodynamic optimization of the shape of the blade, and the other is the increasing length of the blades [15, 17, 27].

In general the aerodynamic optimization of the blade leads to mechanically more complex behavior [26]. The mechanical behavior of optimized rotor blades can, unlike the behavior of previously designed rotor blades not sufficiently be described with simple beam theory and requires more sophisticated models [25]. In addition to this, longer blades lead to higher loads and therefore a more considerate mechanical approach becomes necessary.

The wind turbine rotor blade that will be investigated in the following was designed with the intention of a geometrical bend-twist coupling to passively reduce loads during operation. Modal data from experimental vibration testing and finite element (FE) simulations usually lead to different results. In order to get reliable experimental data, various measures were taken [18]. To get an overview of the structural behavior, broadband random excitation signals are used. To check for specific properties, this is followed by tuned sine excitation. Different excitation levels are chosen, to identify possible nonlinearities. The modal parameters from all excitation runs (high force, low force, random, sine sweep - each in edge-wise as well as flap-wise direction) are compared with each other to extract the "best" modes for the experimental modal model. Modeling errors in simulations can be classified in three main categories: idealization errors, discretization errors and erroneous parameters assumptions [22]. Neither idealization errors nor discretization errors are within the scope of conventional computational model updating [22]. Assuming these errors are negligible, a tuning (updating) of the parameters, so that similar results are achieved is reasonable [5]. The model updating is relying on previously acquired high-fidelity test-data described in [11, 13] and an existing FE model of the wind turbine rotor blade [30, 31]. From Figure 1 an impression of the fixed-free experimental set-up as well as the corresponding FE model can be gained. The model updating in this study is achieved

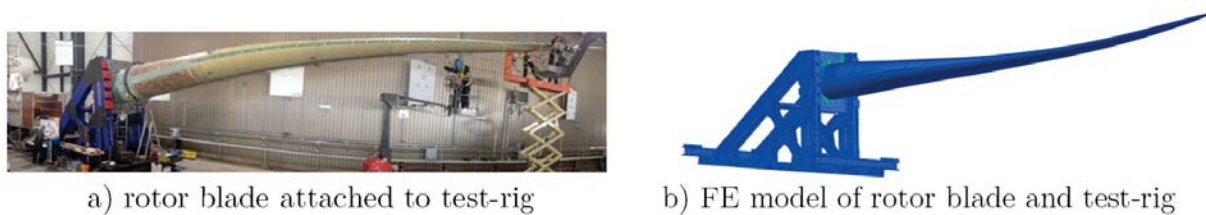a) rotor blade attached to test-rig   b) FE model of rotor blade and test-rig

Figure 1: Experimental setup and FE model

with FEMtools and MSC Nastran.

A simulation model that closer resembles reality will allow for better strain and deflection predictions and therefore offers several advantages. In operations, having better strain estimates leads to better fatigue and life-cycle estimations. Furthermore structural improvements of the mechanical behavior of new blades in the future can be based on a more precise predecessor model. This allows for reduced security margins, as the certainty in the mechanical behavior

of the precursor is higher. Increasing the validity of the deflection predictions enables better assessment of loads on the blade as well as on the entire wind turbine. Finally having more accurate deflection predictions also leads to better estimates of the output electrical power. Numerous publications deal with iterative gradient-based model updating in the aerospace sector whereas only a few publications deal with the model updating of wind turbine blades. One reason for that appears to be, that the security requirements in the aerospace industry are higher than in the wind turbine industry. This is reflected in the certification process. Ground Vibration Tests are necessary for new aircraft prototypes, whereas they are not explicitly recommended for new wind turbine blades [2]. In this context the following publication presents a case study of the updating of a helicopter frame [22], [6] describes the updating of a full scale aircraft and among many others [7, 12, 21, 28] deal with small scale model updating problems. MOGRAVE and FRIBERG treat both a small scale and an industrial sized example [21]. Herein small refers to the dimensions of the model and not necessarily to the number of elements in the FE model. In recent years, some authors dealt with model updating of wind turbine blades. Amongst them [8, 9, 29] focused on a few modes and static deflection data. LUCZAK et al. investigated a blade section and chose a response surface based approach, that led to slightly improved correlation between test and analysis [20]. GROSS et al. updated a small scale wind turbine rotor blade (i.e. small in terms of rotor length) iteratively and sensitivity based [10]. The wind turbine rotor blade is tested under different boundary conditions. The exact improvements achieved with the model updating in terms of correlation between measured and simulated mode shapes remain unclear. In [5] the importance of having fewer parameters than responses and thus creating an (over-) determined system of equations is underlined. While DASCOTTE acknowledges the advantages of such a parameterization, the benefits of using more parameters than responses are described [1].

1.2   Methodology and Structure

The aim of this work is to improve and validate an existing FE model which is directly based on production drawings. In order to achieve this, high fidelity experimental results are used. A brief overview over the existing theoretical foundation for the techniques used in this work is given in Section 2. After an initial comparison of experimental and simulated results, it becomes apparent, that the compliance of the test-rig used during the experiments is non negligible, the model is thus (successfully) manually adapted (Section 3). The global similarity between experimental and simulated results ought to be minimized by adapting material parameters, while reflecting the true properties of the material as close as possible. This is firstly examined with the full set of sensors. A particular focus is laid on minimizing differences between experimental and simulated eigenfrequencies. Furthermore, two different parameterizations are investigated. These parameterizations are used and compared with respect to their advantages and disadvantages (Section 4.1). The parameterization which yields better results is used in the following computational model updating of the wind turbine rotor blade with subsets of sensors. The results of this are compared to the reference case that uses a full set of sensors (Section 4.2). Due to the comprehensive previously acquired experimental data [11], the updated wind turbine rotor blade models can be validated by changing the respective boundary conditions to "free-free" and comparing the results to the respective experimental data set (Section 4.3). In Section 5 the results are summarized and an outlook is given. Section 6 acknowledges the support of different partners, without whom this study would not have been possible. The present work relies on a previously created simulation-model [30] as well as experimental data [11, 13] and is directly based on the study described in [18].

2 Iterative gradient-based model updating

The exact relation between changes in physical quantities like mass and stiffness (i.e. parameters) and the resulting changes in modal properties (i.e. responses) is simple to derive for very small systems but becomes increasingly difficult and practically impossible for industrial sized models. In light of this, the functional relation between parameters and responses is approximated with a TAYLOR series limited to the first two terms

$$
\boldsymbol{r}_{\mathrm{fe}}\left(\boldsymbol{p}\right) = \boldsymbol{r}_{\mathrm{fe}}\left(\boldsymbol{p}_{\mathrm{n}}\right) + \underbrace{\frac{\partial \boldsymbol{r}_{\mathrm{fe}}}{\partial \boldsymbol{p}}\bigg|_{\boldsymbol{p}=\boldsymbol{p}_{\mathrm{n}}}}_{:=\boldsymbol{S}} \left(\boldsymbol{p} - \boldsymbol{p}_{\mathrm{n}}\right). \tag{1}
$$

In this $\boldsymbol{r}_{\mathrm{fe}}$ is the response dependent on the parameters. Responses are chosen by the analyst and comprise (in the context of this work) of mode shapes and derived metrics, eigenfrequencies, mass and center of gravity resulting from the simulation model. $\boldsymbol{p}$ are the parameters (e.g mass and stiffness) and $\boldsymbol{p}_{\mathrm{n}}$ are the parameter values at which the TAYLOR series is evaluated. $\boldsymbol{S}$ stands for the sensitivity of the numerical model. Evaluating $\boldsymbol{r}_{\mathrm{fe}}$ at, yet to determine, new parameter values $\boldsymbol{p}_{\mathrm{n+1}}$, the difference between experimental and numerical responses is

$$
\boldsymbol{\varepsilon} = \boldsymbol{r}_{\mathrm{exp}} - \boldsymbol{r}_{\mathrm{fe}}\left(\boldsymbol{p}_{\mathrm{n+1}}\right) \tag{2}
$$

using the TAYLOR series for $\boldsymbol{r}_{\mathrm{fe}}\left(\boldsymbol{p}_{\mathrm{n+1}}\right)$ leads to the error term

$$
\boldsymbol{\varepsilon} = \underbrace{\boldsymbol{r}_{\mathrm{exp}} - \boldsymbol{r}_{\mathrm{fe}}\left(\boldsymbol{p}_{\mathrm{n}}\right)}_{:=\Delta \boldsymbol{r}} - \boldsymbol{S} \underbrace{\left(\boldsymbol{p}_{\mathrm{n+1}} - \boldsymbol{p}_{\mathrm{n}}\right)}_{:=\Delta \boldsymbol{p}}. \tag{3}
$$

The objective function is then defined as

$$
J(\Delta \boldsymbol{p}) = \boldsymbol{\varepsilon}^T \boldsymbol{W}_r \boldsymbol{\varepsilon} + \Delta \boldsymbol{p}^T \boldsymbol{W}_p \Delta \boldsymbol{p}. \tag{4}
$$

It is dependent on the parameter changes $\Delta \boldsymbol{p} = \left(\boldsymbol{p}_{\mathrm{n+1}} - \boldsymbol{p}_{\mathrm{n}}\right)$. By additionally introducing diagonal weighting matrices for the parameters ($\boldsymbol{W}_p$) and the responses ($\boldsymbol{W}_r$) confidence in both experimental results and numerical model assumptions can be expressed [1]. The weighting matrices furthermore have a regularizing effect, which is comparable to a TIKHONOV-regularization [5]. Minimizing (4) leads to the calculation formulae for the new parameter $\boldsymbol{p}_{\mathrm{n+1}}$ as defined in [1] and given in the following. According to DASCOTTE [1], if the number of parameters is less than or equal to the number of responses the new parameter values are calculated as

$$
\boldsymbol{p}_{\mathrm{n+1}} = \boldsymbol{p}_{\mathrm{n}} + \left(\boldsymbol{W}_p + \boldsymbol{S}^T \boldsymbol{W}_R \boldsymbol{S}\right)^{-1} \boldsymbol{S}^T \boldsymbol{W}_R \Delta \boldsymbol{r}, \tag{5}
$$

if the number of parameters is larger than the number of responses the new parameters are calculated with the equation

$$
\boldsymbol{p}_{\mathrm{n+1}} = \boldsymbol{p}_{\mathrm{n}} + \left(\boldsymbol{W}_P\right)^{-1} \boldsymbol{S}^T \left(\boldsymbol{W}_R^{-1} + \boldsymbol{S} \boldsymbol{W}_P^{-1} \boldsymbol{S}^T\right)^{-1} \Delta \boldsymbol{r}. \tag{6}
$$

2.1 Unification of measurements and simulations

In preparation of the updating, measurements and simulations have to be unified in many respects, which will be described in the following. Within this work all mode shapes (i.e experimental mode shapes ψ_r and simulated mode shapes ϕ_r) are scaled to largest component one. In the following damping is not considered and therefore the numerically calculated mode

shapes are entirely real valued. As the blade is lightly damped [18] using the magnitude and an appropriate sign for the experimental results as described in [1] is reasonable. In order to compare measurements and numeric calculations a common set of measurement points and degrees of freedom (DOFs) must be chosen. The numeric results can be reduced to the measurement points and DOFs, or the measurements can be expanded to the numerical calculated points and degrees of freedom. Expanding the measurement results implies interpolation between measurement points and can for example be achieved with the system equivalent reduction and expansion process (SEREP as described in [24]). To reduce the simulation results, the measurement points of the structure are mapped to nearby FE nodes. This means, that the results at DOFs, that are not close to a measurement point are omitted. As there are usually significantly more nodes than measurement points, the number of deleted results is large. The results (i.e. mode shapes) will be reduced to the measurement points.

2.2 Metrics for comparison

After measurements and simulations are unified, the similarity of measurement and simulation results can be quantified. This similarity quantification is helpful in the manual model adaptation and necessary for the computational model updating procedure. In the computational model updating select pairs are formed between experimental modes and simulated modes that have a high initial congruence.

In the derivation of most metrics, model assumptions and mathematical properties, like mass orthogonality or linear independence of eigenvectors are exploited. While the indicators described hereafter are rather similar, an important distinction is whether they refer to every DOF or they are giving a value for all DOFs. The same normal mode shapes have to be collinear and different mode shapes must be orthogonal with respect to the mass matrix [3]. This is supposed to be true for (normalized) experimental modes, numerical modes and between numerical and (normalized) experimental modes. Due to inaccurate and incomplete measurements, this relation is in practice not entirely fulfilled. Besides using Mass M as a weighting factor one can also directly check the orthogonality of mode shapes. The Mass Matrix M can (like any model of the real world) only be approximately correct. It is therefore reasonable to use no weighting factor instead of using a potentially wrong weighting factor. One then calculates the modal-assurance-criterion (MAC) for the simulated mode ϕ_k (with the numbering k) and the experimental mode ψ_m (with the numbering m):

$$\text{MAC}(\phi_k, \psi_m) = \frac{\left(\phi_k^T \cdot \psi_m\right)^2}{\left(\phi_k^T \cdot \phi_k\right)\left(\psi_m^T \cdot \psi_m\right)}. \tag{7}$$

The resulting value is $100\,\%$ for collinear modes and $0\,\%$ for orthogonal modes [1]. MAC values between simulated mode shapes of the same simulation are, as MAC value between experimental mode shapes of the same dataset, referred to as AUTOMAC values. As a measure of orthogonality for every degree of freedom l, over N mode shapes (with the numbering k) the coordinate-modal-assurance-criterion (COMAC) is introduced [1]

$$\text{COMAC}(l) = \frac{\left(\sum_{k=1}^{N} (\phi)_k^l \, (\psi)_k^l\right)^2}{\left(\sum_{k=1}^{N} (\phi)_k^l \, (\phi)_k^l\right)\left(\sum_{k=1}^{N} (\psi)_k^l \, (\psi)_k^l\right)}. \tag{8}$$

The COMAC gives a sum (and therefore allows for fast checks) for multiple modes. The COMAC takes values between zero and one hundred percent. For brevity, the percentage signs are oftentimes omitted in the following.

3   Comparison of initial results and manual model adaptation

In Figure 2 the eight initially paired mode shapes are shown. In this figure, the experimental results are shown in red, while the simulated results are shown in blue. Their medium MAC value of 92 and medium frequency deviation of 8.8 % is detailed in Figure 6. It is noteworthy that mode shape 2.) has a MAC value of 98 inspite of its dissimilar appearance in Figure 2 2.). This is due to the fact, that sensors in edge-wise direction are only installed on the leading edge (Fig. 13 2.)), therefore the test-model (red) is not deformed in edge-wise direction at the other positions. It becomes apparent, that for all mode shape pairs apart from the first one, the experimentally determined eigenfrequency is higher than the simulated eigenfrequency. Furthermore the overall MAC values are high, but decrease slightly for modes with higher frequency.
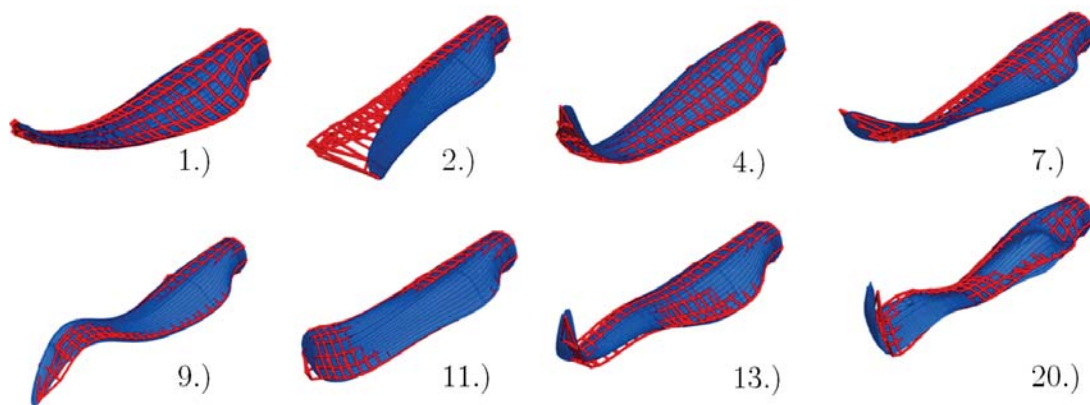
Figure 2: Initially paired mode shapes (numbered according to experimental mode shape number)
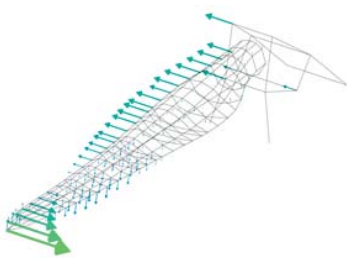
Figure 3: rig-mode at 7.2 Hz

The blade is tested while being clamped to a test-rig Figure 5 a). In a first approach a fixed-boundary condition is applied (i.e. displacement and rotations in all directions are suppressed) at the first nodal line on the blade root. An inspection of the COMAC values displayed in Fig. 4 a) and Fig. 4 b shows, that the local correlation gets significantly lower towards the root of the blade. Herein the gray markers indicate COMAC values below 50. In Figure 3 the first (experimental) rig-mode is depicted. Since this is the fifth experimental mode, it is concluded that the compliance of the test-rig is non negligible and therefore an FE model of the test-rig is created. The FE model of the blade is then rigidly attached to the FE model of the test-rig. The test-rig is made out of steel. The exact sort of the steel is unknown to the authors, S335 with its properties given in e.g. [4] is used in the model. To efficiently simulate the behavior of the test-rig, small features, like chamfers, holes and bolts are removed from the model. The simplified geometry of the test-rig is shown in Figure 5 b. Based on the simplified geometry, with unstructured meshing an FE model that consists of 58398 CTETRA-elements is constructed. The test-rig is estimated to have total mass of 23.5 tons. Removing holes, bolts and chamfers leads to an increase in mass of 1.5 tons and an (not quantified) increase in stiffness. The test-rig is fixed to the ground at four corner points with threaded rods. Nonetheless, the test-rig is assumed to move in lateral direction. This assumption is backed by the width of the support surface of the H beam (as depicted in the bottom
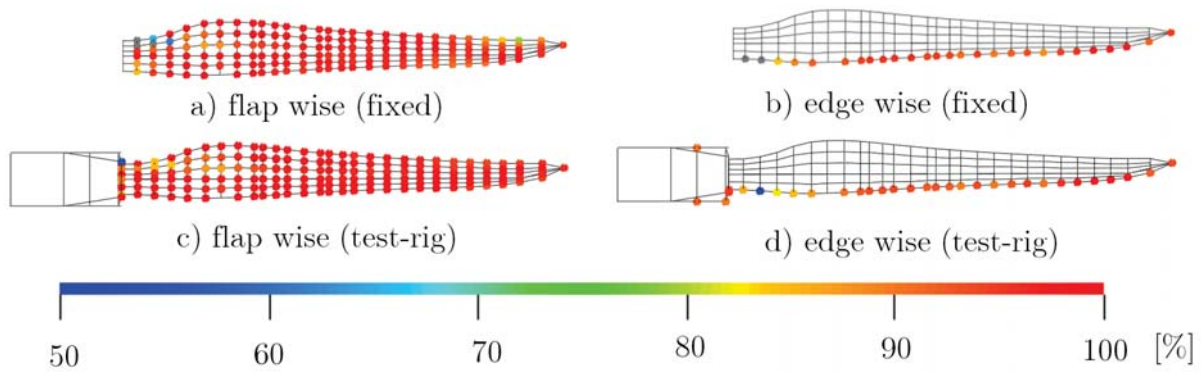
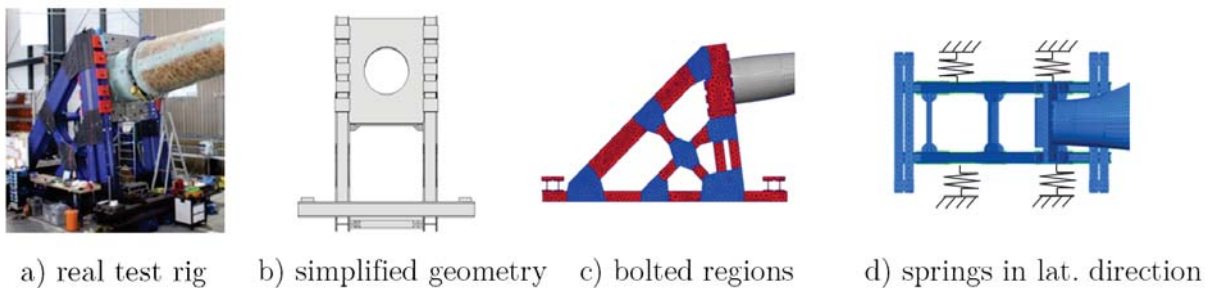Figure 4: COMAC for 8 initially paired mode shapes

Figure 5: Test-rig: from reality to FE-model

of Fig. 5 a) and Fig. 5 b)) on which the test-rig stands (1 cm for each surface, therefore 4 cm in total). This assumed lateral movement is described in the model, by attaching springs in lateral direction at every node on the bottom surfaces of the H beams (as symbolized in Fig. 5 d). The spring constants as well as the stiffness of the test-rig in areas of bolted connections shown in blue in Figure 5 c) are adjusted to reproduce the first rig-mode. With a stiffness reduction in these areas to 10 % of the nominal stiffness, a MAC value of 85 % and a frequency deviation of 1.64 % deviation is reached for the simulated mode and the experimental mode displayed in Figure 3. Furthermore, significantly higher COMAC values are reached for the initially paired mode shapes in both flap wise (Fig. 4 c)) and edge wise direction (Fig. 4 d)). Since the COMAC is calculated over all initially paired mode shapes, the increased COMAC values indicate, that the test-rig describes the reality more closely, than a fully fixed boundary condition. In Figure 6, MAC values as well as frequency deviations between simulated and experimental results for both the initial configuration (i.e. fully fixed) and the configuration with the auxiliary test-rig are shown. From this, it becomes clear, that the simulation model with the auxiliary test-rig not only leads to increased MAC values (compared to the initial configuration) but also three mode shapes (5.) 18.) 19.)) that where previously not paired (n.p.) and are now paired. Despite the slightly increased deviations in eigenfrequency for the model with the auxiliary test-rig (Fig. 6 c)), the overall similarity between experiment and simulation is increased with the above described manual model adaptation.

4   Computational Model updating

In order to further improve the global similarity between simulated and experimental results the model of the blade is computationally updated as described in the following. In this process the above described auxiliary model of the test-rig is used but not further adapted.
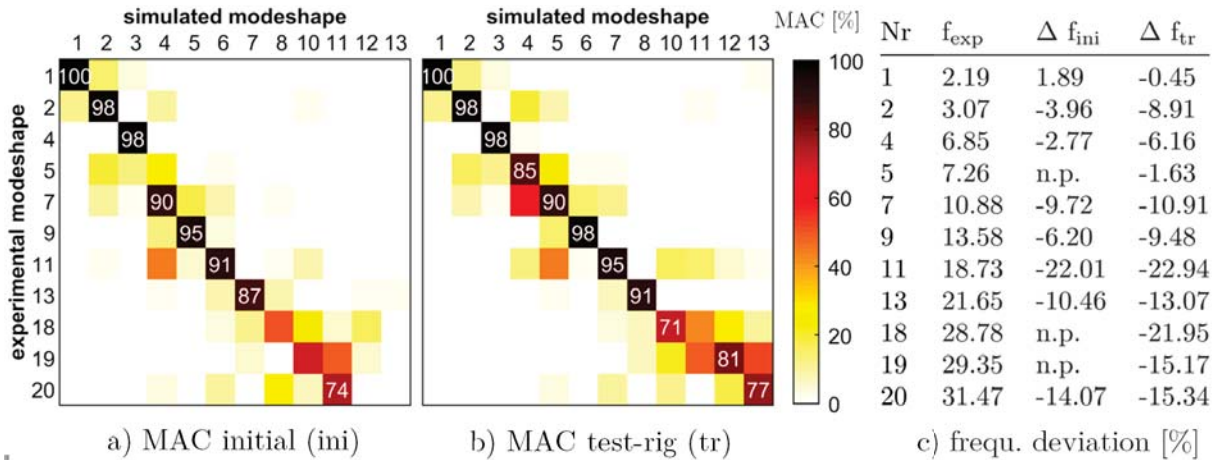
Figure 6: MAC and deviation in eigenfrequency for initial and manually adapted model

Nr	f_{exp}	Δf_{ini}	Δf_{tr}
1	2.19	1.89	-0.45
2	3.07	-3.96	-8.91
4	6.85	-2.77	-6.16
5	7.26	n.p.	-1.63
7	10.88	-9.72	-10.91
9	13.58	-6.20	-9.48
11	18.73	-22.01	-22.94
13	21.65	-10.46	-13.07
18	28.78	n.p.	-21.95
19	29.35	n.p.	-15.17
20	31.47	-14.07	-15.34

c) frequ. deviation [%]

4.1 Updating based on full set of sensors - reference configuration

4.1.1 Responses

The magnitude of the relative deviation in eigenfrequency $|\Delta f| = |(f_{fe}-f_{exp})/f_{exp}|$ between a simulated (fe) and an experimental mode (exp) is used as one measure for pairing respective modes. This is due to the fact that, in conjunction with similar mode shapes, this deviation is a good indicator of similarity and therefore helps in relating models in terms of their dynamic behavior. In the following, experimental and simulated modes are considered to be paired, if they have MAC value above 70 % and an absolute frequency deviation of less than 30 %.

As responses MAC values (11) and frequency deviations (11) of paired mode shapes as well as the center of gravity (1) in spanwise direction (COG) and the mass (1) are used. This results in a total number of 24 responses. The responses are weighed differently. The diagonal response weighting matrices W_R are built from the weights as given in the following. The frequency responses are, as oppose to all other responses which are given a weighting of 1, given different weights in the objective function (Tab. 4.1.1). Responses with higher weights are emphasized in the objective function, while responses with a lower weight are not. The weighting is based on the premise, that in the updating of this rotorblade, large initial discrepancies in frequency (in particular for torsional modes) ought to be minimized, while mode shape correlation should improve.

Table 1: response weighting

Experimental Mode Shape	1.)	2.)	4.)	5.)	7.)	9.)	11.)	13.)	18.)	19.)	20.)
frequency weighting	1	2	1	1	2	1	4	1	2	2	4

4.1.2 Initial sensitivities

To tune the global dynamic behavior of the simulation model, two types of parameters are used. A scaling factor on the membrane stiffness as well as a scaling factor on the density. In preparation of the parameterization, sensitivities are calculated for every shell element with respect to each response. The summed normalized initial sensitivities are displayed in Figure

7. Herein the scale is limited to allow the detection of relevant regions. For a small number of elements the magnitude of the sensitivities is larger than shown in Figure 7. With this, it becomes apparent that different regions are particularly sensitive. It is worth noting, that apart from the areas marked in red and blue in Figure 7, the beginning of the spar (not visible in the figure) is highly sensitive to changes in density as well as in membrane stiffness.
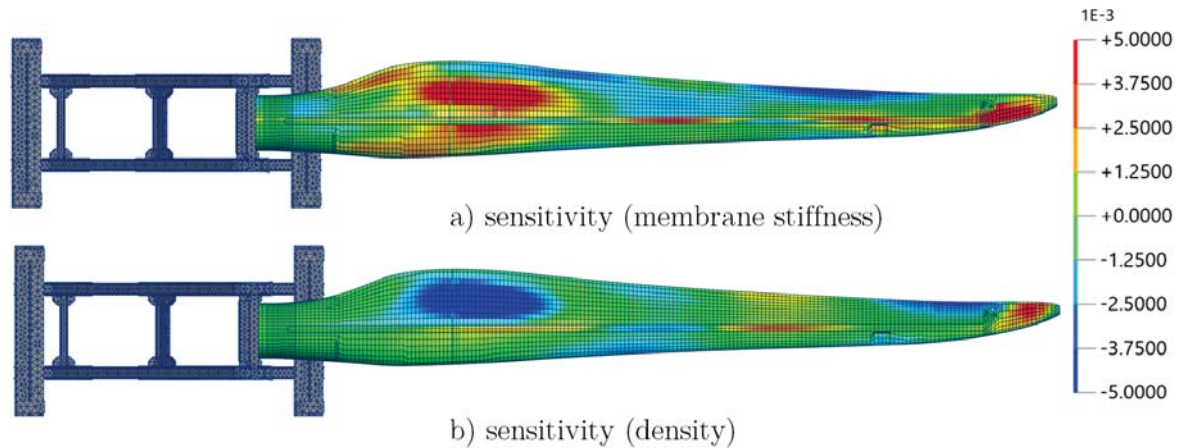

Figure 7: Initial summed normalized sensitivities (limited scale)

4.1.3 Parameterization

The model is parameterized in two different ways. In the first approach 12 design fields are used. Using one scaling factor on the membrane stiffness and one scaling factor on the density as parameters for each design field leads to 24 parameters in total. The design fields are equally spaced from root to tip and numbered consecutively from left to right, beginning in the upper left and ending in the lower right (Fig. 8 a)). The spar is included in the lower 6 design fields (i.e. design field number 7 to design field number 12). In the second approach 40 design fields as shown in Figure 8 b) are used and numbered according to the same scheme as in the other parameterization. Additionally 19 design fields are equally spaced along the spar (from root to tip) leading to a total number of 59 design fields and thus 118 parameters. The first parameterization has the advantage of using the same number of parameters (24) as responses (24) and therefore leading to a determined system of equations. In spite of this drawback, the parameterization with 118 parameters has the advantage of a finer spatial resolution and furthermore accounts for differences in sensitivities on the spar as oppose to the outer hull of the blade. Since the second parameterization uses fewer responses than parameters, the parameter changes are additionally constrained to their initial value in order to ensure a deterministic updating procedure. Because the model is directly based on production drawings, the maximum
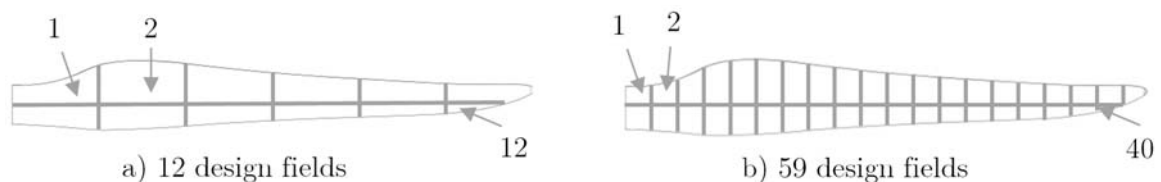

Figure 8: Design fields leading to parameterizations

parameter change is set to 15%. While the exact number is based on engineering judgment, the general limitation of parameter changes is due to the notion, that the updated model should not just reproduce the experimental results but also reflect the true material properties as close as possible [23]. The parameter change per iteration is limited to 0.5 % in order achieve a smooth convergence of parameters. All parameters are weighed equally with a value of 1 (i.e. $\boldsymbol{W}_P$ is the identity matrix). This is due to the fact, that there is no indication of particular uncertainty on select parameters.

4.1.4 Adaptations

The parameters are adjusted in 150 iteration steps. The final parameter values are shown in Figure 9. Both models are adapted similarly. This is particularly the case for the membrane stiffness (Fig. 9 c), Fig. 9 d)) where the membrane stiffness in large regions is increased by the set maximum of 15 %. Figure 9 b) shows, that the density at the tip of the blade is changed significantly differently in the two neighboring design fields 19 and 20. The discrepancy of more than 20 % shows that using a finer spatial resolution is particularly reasonable in this area. Furthermore, the differences between the adaptations of the spar as oppose to the outer hull of the blade (Figure 9 b) Figure 9 d)) indicates, that the sensitivities throughout the updating process differed. Since, in the parameterization with 12 design fields, the spar is included in the design fields towards the leading edge, the adaptations to the spar shown in Fig. 9 a) b) are equal to the respective parameter changes for the outer hull of the blade. Figure 10 shows
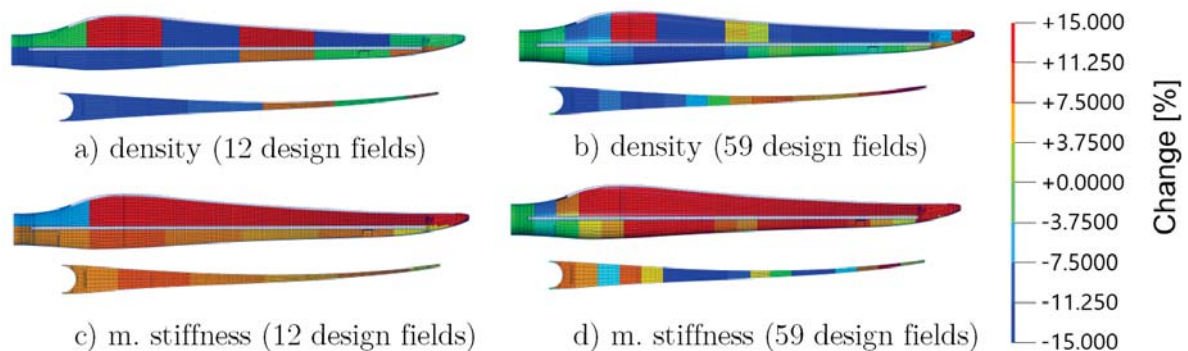

Figure 9: Parameter adaptations after 150 iteration steps

the parameter evolution over 150 iteration steps. Numerous parameters are increased to the set magnitude limit of 15% change after a comparatively small number of iterations. Besides this, parameters do not visibly change slope of change (i.e. parameters that decrease in the beginning continue to decrease and parameters that increase in the beginning continue to increase).

4.1.5 Results

Oposing Figure 6 and Figure 11 highlights, that updating the FE model (while using the FE model of the test-rig) leads to increased MAC values and decreased frequency deviations. Figure 11 a) and b) show that the MAC values are improved with both parameterizations. The parameterization with 118 parameters leads to an (overall) higher similarity (i.e. increased MAC values and decreased frequency deviations) than the parameterization with 24 parameters (Fig. 11) . From Figure 12 it becomes clear, that the parameter adaptations lead to an improvement
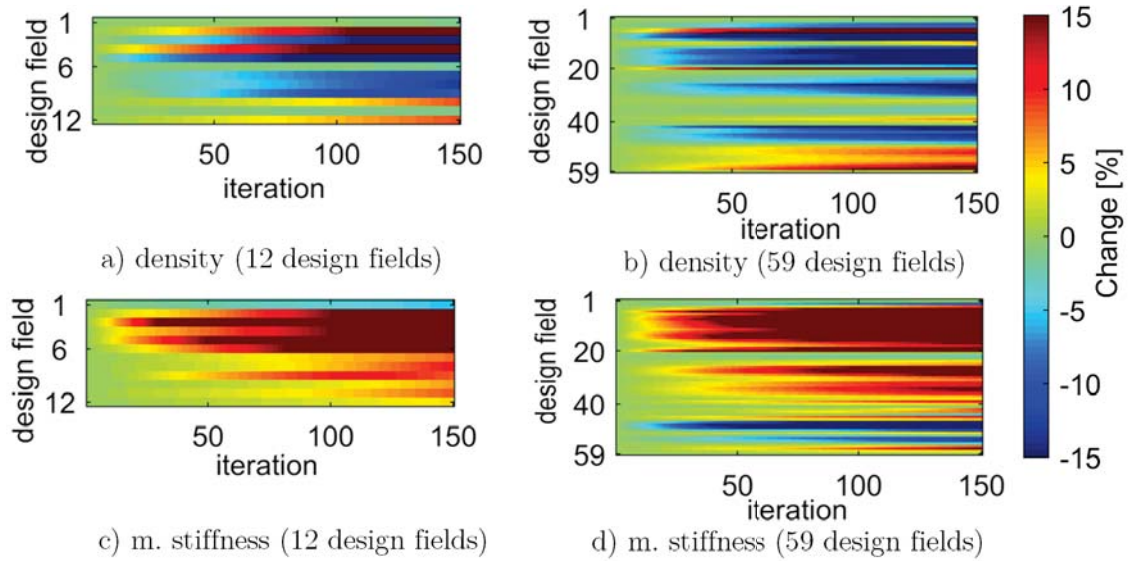
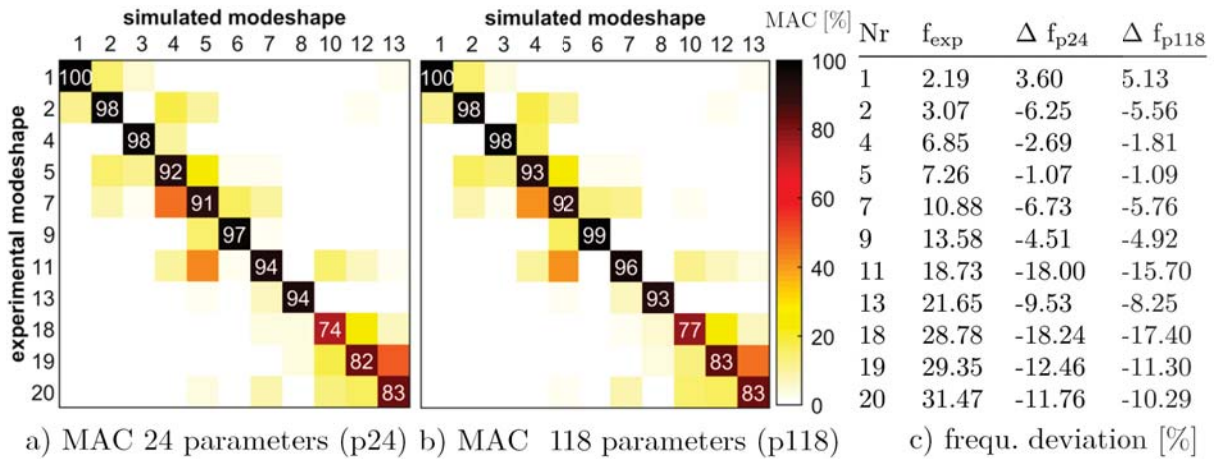Figure 10: Evolution of iteratively adapted parameters

Figure 11: MAC and deviation in eigenfrequency for updated models

in mean MAC value and decreasing discrepancy in frequency. Furthermore Figure 12 shows, that these similarity indicators are better for the parameterization with 118 parameters than for the parameterization with 24 parameters. It ought to be noted, that, while frequency deviations are still decreasing after iteration 100 mean MAC values are slightly deteriorating.

4.2 Updating based on reduced set of sensors

The updating with the reduced set of sensors uses the sensor locations shown in Figure 13 and is performed with the second parameterization (i.e. 118 parameters), which yielded better results in the reference case. The updating is performed with different sets of sensors selections. While the number of sensors used in the updating is reduced, the modal model is not changed, i.e. the modal identification is not repeated with the reduced sensor sets. The full set of sensors is displayed in green in the upper part of Figure 13. The total number of paired sensors on the wind turbine rotor blade and the test-rig is 272, 237 sensors are in flap wise direction while 35 are in edge wise direction (at the leading edge). The number of sensors is iteratively reduced. In each step one sensor is removed based on the notion, that the sum over the off-diagonal values of
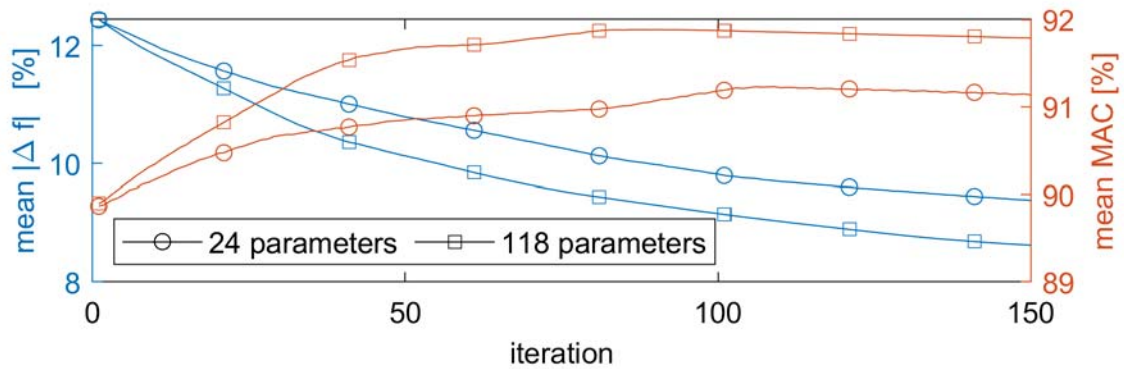
Figure 12: Evolution of medium MAC value and frequency deviation

the AUTOMAC-matrix for the Finite-Element (FE) mode shapes 1 to 20 evaluated at the sensor positions is minimized. Three configurations with reduced sensor sets will be investigated. The number of sensors is reduced to 1/2 (red. sens (1/2)), 1/4 (red. sens. (1/4)) and 1/8 (red. sens. (1/8)). The remaining sensors for these configurations are marked on the lower test-model in Figure 13. In the first configuration, sensors are located at all color-marked positions (red. sens (1/2)), the second configuration uses only the sensors at the positions marked in yellow and red (red. sens. (1/4). The third configuration uses only sensors at the locations marked in yellow (red. sens (1/8)). From Figure 14 it becomes clear, that potentially hard to distinguish mode shapes e.g. 11 and 12 are hard to distinguish for all configurations. Overall the AUTOMAC matrices lead to the impression, that most mode shapes up to the 20th mode are well distinguishable for all configurations. The evolution of the mean similarity indicators
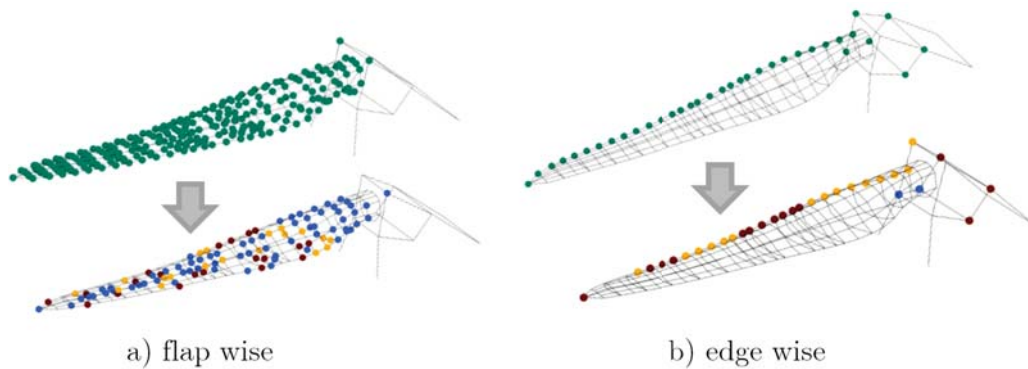

Figure 13: Full and reduced sensor selection

for the updating of these reduced configurations are displayed in Figure 15. It becomes clear, that the frequency discrepancy for all reduced sensor configurations is minimized as well as for the full sensor configuration. In contrast to this, the MAC improvements for the reduced configurations (red. sens. (1/4) and (red. sens. (1/8))) are smaller than for the full set of sensors or nonexistent (red. sens. (1/2)).

4.3 Verification

The boundary condition of the updated models is changed to "free-free" and compared to the experimental "free-free" modal-data described in [11]. An overview of these verification results can be gained from Figure 16. In this, the similarity metrics are calculated for mode
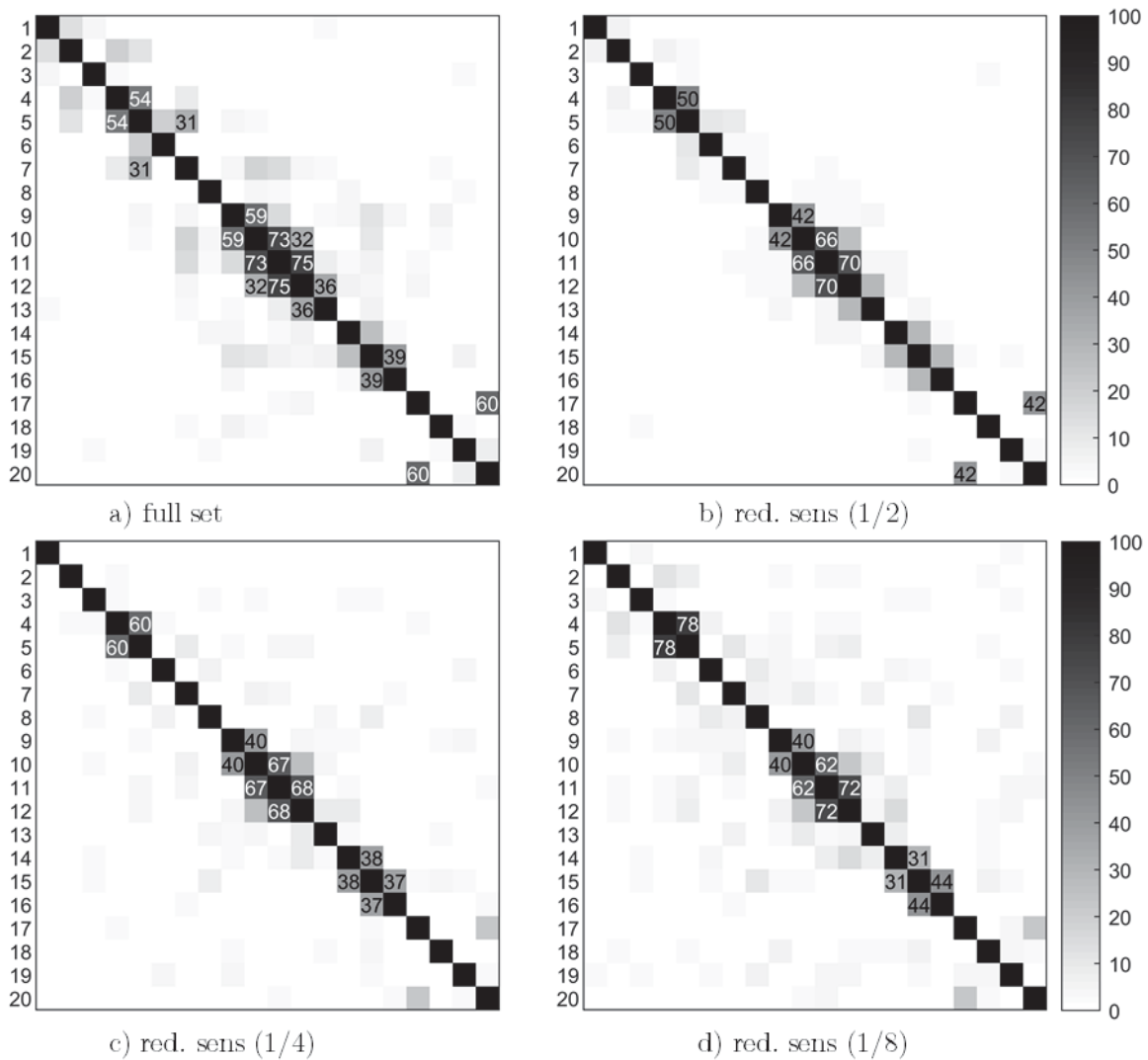
Figure 14: FE-AUTOMAC matrices in [%] evaluated for full and reduced sensor sets

shape pairs that occur in all configurations. It becomes clear, that the mean frequency deviation is improved for all configurations and all mean MAC values are marginally aggravated. The improvements are slightly better in terms of the MAC values for the parameterization with 24 parameters as oppose to the parameterization with 118 parameters. With respect to the mean frequency deviation, the parameterization with 118 parameters leads to slightly better results.

5 Summary and Outlook

In the present work, several aspects of the model updating of an industrial-sized FE model of a wind turbine rotor-blade were investigated. The more accurate representation of the boundary condition by creation of an auxiliary FE model led to the largest improvement in MAC values and slightly worsened the frequency deviation. In this case study, a parameterization with a number of parameters that exceeds the number of responses led to better results, than a parameterization in which the number of parameters is equal to the number of responses (Fig. 11). Furthermore it was shown, that with a reduced number of sensors, the frequency deviation can be minimized well, while the correlation of the MAC values was not significantly improved
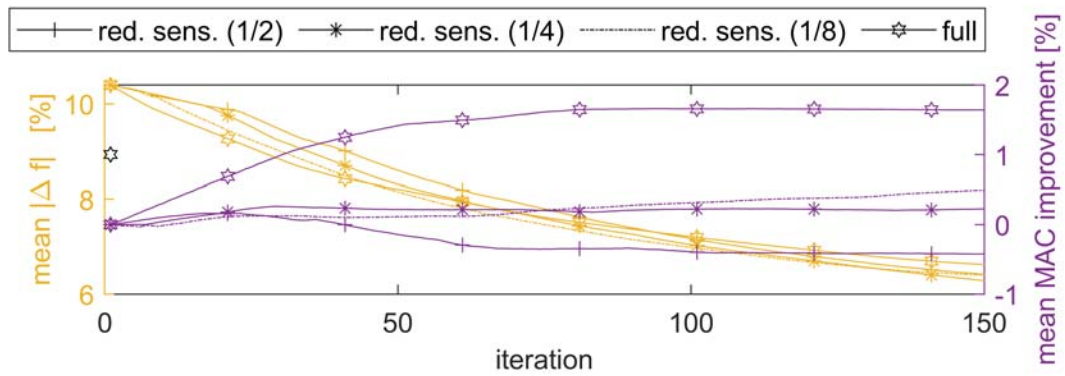
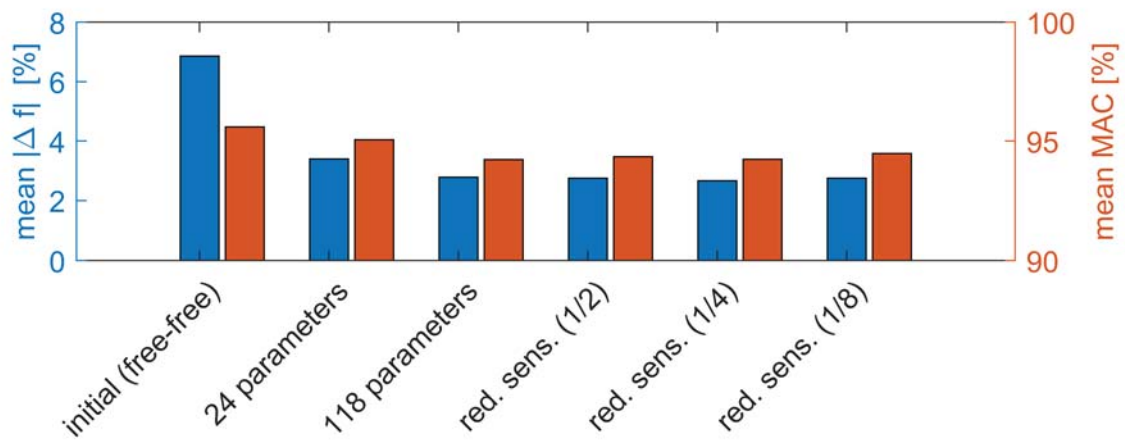Figure 15: Evolution of similarity criteria for reduced sensor sets

Figure 16: Verification of Updating results under altered boundary condition

(Fig. 15). The evolution of parameters showed no obvious ripple effects, which indicates, that the step-size for the parameter adjustments was chosen to be small enough. A large number of parameters was at the set global limit of 15%. Relevant parameter changes where observed for almost all parameters. While the observed improvements are in line with the focus on decreasing frequency deviations, it becomes apparent, that the parameter adaptations do not fully represent the true material characteristics. In light of this, future works should use different parameterizations and judge the respective results. If mode shape correlation improvements are of interest, a large number of sensors should be used. The effects of response-weighting are assumed to be relevant and will be examined in future works.

6 Acknowledgments

References

[1] E. Dascotte. FEMtools Model Updating Theoretical Manual. June 2019.

[2] DIN EN 61400-23:2014-12;VDE 0127-23:2014-12. Wind energy generation systems - part 23: rotor blades, 2019.

[3] D. Ewins. *Modal testing: theory and practice*, volume 15. Research studies press Letchworth, 1984.

[4] U. Fischer. *Tabellenbuch metall (mit Formelsammlung)*. Europa-Lehrmittel, 2011.

[5] M. Friswell and J.E. Mottershead. *Finite Element Model Updating in Structural Dynamics*. Solid Mechanics and Its Applications. Springer Netherlands, 2013. ISBN 9789401585088.

[6] D. Göge. Automatic updating of large aircraft models using experimental data from ground vibration testing. *Aerospace Science and Technology*, 7(1):33 – 45, 2003. ISSN 1270-9638. doi:https://doi.org/10.1016/S1270-9638(02)01184-7.

[7] Y. Govers. *Parameter identification of structural dynamic models by inverse statistical analysis*. PhD thesis, Universitätsbibliothek Kassel, 2012.

[8] D. Griffith and T. Carne. Experimental modal analysis of 9-meter research-sized wind turbine blades. In *Structural Dynamics and Renewable Energy, Volume 1*, pages 1–14. Springer, 2011.

[9] T. Griffith, J. Paquette, and T. Carne. Development of validated blade structural models. In *46th AIAA Aerospace Sciences Meeting and Exhibit*, page 1297, 2008.

[10] Johann Gross, Tobias Oberhardt, Pascal Reuss, and Lothar Gaul. Model updating of the ampair wind turbine substructures. In *32nd International Modal Analysis Conference (IMAC XXXII)*, 2014.

[11] J. Gundlach and Y. Govers. Experimental modal analysis of aeroelastic tailored rotor blades in different boundary conditions. In *Journal of Physics: Conference Series*, volume 1356, page 012023. IOP Publishing, 2019.

[12] A. Gupta, C. Moreno, H. Pfifer, B. Taylor, and G. Balas. Updating a finite element based structural model of a small flexible aircraft. In *AIAA Modeling and Simulation Technologies Conference*, page 0903, 2015.

[13] B. Haller. Smartblades2 - deliverable del 1.2.2.1 del 1.2.2.2 del 1.2.2.3 rev. 0.0. 2018.

[14] R. Hara. Chapter 5 - prediction of wind power generation output and network operation. In Toshihisa Funabashi, editor, *Integration of Distributed Energy Resources in Power Systems*, pages 109 – 131. Academic Press, 2016. ISBN 978-0-12-803212-1. doi:https://doi.org/10.1016/B978-0-12-803212-1.00005-2.

[15] C. Hernández, T. Telsnig, and A. Pradas. Jrc wind energy status report 2016 edition. *Market, Technology and Regulatory Aspects of Wind Energy*, 2017.

[16] International Renewable Energy Agency IRENA. Installed capacity trends. https://www.irena.org/win, 2019. Last accessed on 27th of August 2019.

[17] J. Kaldellis and D. Zafirakis. The wind energy (r) evolution: A short review of a long history. *Renewable energy*, 36(7):1887–1901, 2011.

[18] J. Knebusch. Finite element model updating of wind turbine rotor blades using modal data aquired with attached load frames. Master's thesis, Technical University Berlin, 2019.

[19] D. Leung and Y. Yang. Wind energy development and its environmental impact: A review. *Renewable and sustainable energy reviews*, 16(1):1031–1039, 2012.

[20] M. Luczak, S. Manzato, B. Peeters, Kim. Branner, P. Berring, and M. Kahsin. Updating Finite Element Model of a Wind Turbine Blade Section Using Experimental Modal Analysis Results. *Shock and Vibration*, 2014:1–12, 2014. ISSN 1070-9622, 1875-9203. doi:10.1155/2014/684786.

[21] P. Mograve and O. Friberg. Updating large finite element models in structural dynamics. *AIAA journal*, 36(10):1861–1868, 1998.

[22] J. Mottershead, M. Link, and M. Friswell. The sensitivity method in finite element model updating: A tutorial. *Mechanical Systems and Signal Processing*, 25(7):2275–2296, October 2011. ISSN 08883270. doi:10.1016/j.ymssp.2010.10.012.

[23] H. Natke. *Einführung in Theorie und Praxis der Zeitreihen- und Modalanalyse: Identifikation schwingungsfähiger elastomechan. Systeme*. Grundlagen der Ingenieurwissenschaften. Vieweg, Braunschweig, 2., verb. aufl edition, 1988. ISBN 978-3-528-18145-1. OCLC: 246837170.

[24] J. O'Callahan and P. Li. A non smoothing serep process for modal expansion. In *Proceedings of the 12th International Modal Analysis*, volume 2251, page 232, 1994.

[25] W. Ostachowicz, M. McGugan, J. Schröder-Hinrichs, and M. Luczak. *MARE-WINT: new materials and reliability in offshore wind turbine technology*. Springer, 2016.

[26] S. Scott, M. Capuzzi, D. Langston, E. Bossanyi, G. McCann, P. Weaver, and A. Pirrera. Gust response of aeroelastically tailored wind turbines. In *Journal of Physics: Conference Series*, volume 753, page 042006. IOP Publishing, 2016.

[27] J. Serrano-González and R. Lacal-Arántegui. Technological evolution of onshore wind turbines—a market-based analysis. *Wind Energy*, 19(12):2171–2187, 2016.

[28] J. Sinha and M. Friswell. Model updating: a tool for reliable modeling, design modification and diagnosis. *The Shock and Vibration Digest*, 34(1):27–35, 2002.

[29] J. White, D. Adams, and M. Rumsey. Modal analysis of cx-100 rotor blade and micon 65/13 wind turbine. In *Structural Dynamics and Renewable Energy, Volume 1*, pages 15–27. Springer, 2011.

[30] C. Willberg. Smartblades 2 finite element reference wind turbine blade model, 2020. URL `https://doi.org/10.5281/zenodo.3628356`.

[31] C. Willberg. Validation of a 20m wind turbine blade model. *Wind Energy Science*, 2020. Currently under review.